Multi-objective optimization approach to the ALSTOM gasifier problem

I A Griffin*, P Schroder, A J Chipperfield and **P J Fleming**
Department of Automatic Control and Systems Engineering, The University of Sheffield, UK

Abstract: A control system design procedure based on the optimization of multiple objectives is used to realize the control design specifications of the linear gasification plant models. A multi-objective genetic algorithm (MOGA) is used in conjunction with an H_∞ loop-shaping design procedure (LSDP) in order to satisfy the requirements of this critical system. The H_∞ LSDP is used to guarantee the stability and robustness of the controller while its associated weighting matrix parameters are selected using the multi-objective search method in order to achieve performance requirements. A controller emerges which is stable but unable to completely meet some of the control objectives. Despite this shortcoming, the study is an excellent vehicle for introduction to an effective H_∞ loop-shaping procedure. Further work, beyond the scope of this challenge has subsequently produced an improved controller design.

Keywords: H_∞ control system design, multi-objective optimization, genetic algorithms, robustness

NOTATION

$f(x)$	multi-objective function vector
$\mathbf{G}$	open-loop plant transfer function matrix
$\mathbf{G}_d$	disturbance transfer function matrix
$\mathbf{G}_s$	shaped open-loop plant transfer function matrix
H_∞	'H' infinity
$\mathbf{K}$	controller transfer function matrix
$\mathbf{U}$	matrix of output singular vectors
$\mathbf{V}$	matrix of input singular vectors
$\mathbf{W}_1$	pre-plant weighting matrix
$\mathbf{W}_2$	post-plant weighting matrix
x	vector of decision variables
γ	robustness metric
Δ	normalized perturbation
λ	eigenvalue
ρ	spectral radius (largest eigenvalue magnitude)
σ	singular value
$\mathbf{\Sigma}$	diagonal matrix of singular values

The MS was received on 17 July 2000 and was accepted after revision for publication on 27 September 2000.
** Corresponding author: Department of Automatic Control and Systems Engineering, The University of Sheffield, Mappin Street, Sheffield S1 3JD, UK.*

1 H_∞ CONTROL SYSTEM DESIGN METHOD TUNED BY A MULTI-OBJECTIVE GENETIC ALGORITHM

The specified objective for the work summarized in this paper was to perform a controller design procedure for the gasifier described in reference [1]. The nature of the input and output constraints categorize the gasifier as a critical system [2, 3], i.e. a system which requires the error, or other outputs, to remain within strict limits. The aim of the control system designer is to ensure that these critical limits are not breached due to the presence of disturbances or changes in the system inputs. The basis of the chosen controller design method is the H_∞ loop-shaping design procedure (LSDP) of MacFarlane and Glover [4] and Glover and MacFarlane [5]. This technique is used in conjunction with a multi-objective genetic algorithm (MOGA) [6] to produce a powerful controller design strategy.

1.1 H_∞ design process

H_∞ control system design is an optimization-based controller design technique. Recent research has reported that the technique has been applied in a number of areas, notably aerospace [7–9]. It offers the designer a method which can handle multi-variable as well as single-loop systems. Levels of robustness can be specified and trade-

offs between performance and robustness in the design procedure can be incorporated. The technique utilizes the related concepts of singular values and the H_∞ norm, the latter being defined for the transfer function matrix **G**:

$$\| \mathbf{G}(s) \|_\infty = \max_\omega [\bar{\sigma}(G(j\omega))] \quad (1)$$

where $\sigma(\cdot)$ denotes the singular values and $\| \cdot \|_\infty$ denotes the H_∞ norm.

Classical controller design addresses the robustness concerns using gain and phase margin settings. Interactions present in cross-coupled multi-variable systems render these methods unreliable as indicators of system robustness. Instead, model uncertainty is incorporated into the design process by representing the plant using a nominal model augmented by a model of the possible uncertainty or disturbance. The controller strategy is to maximize the size of the modelling error that can be tolerated while retaining closed-loop stability. In other words, the design procedure seeks to stabilize the set of possible systems that could result from the uncertainty in the plant representation. This is achieved by minimizing the H_∞ norm of the reciprocal of the modelling error.

Performance requirements are addressed through the shaping of frequency responses. This is achieved by using weighting function matrices to provide an acceptable trade-off between disturbance rejection, noise attenuation and the minimization of control energy. The usual mechanism for doing this is the minimization of the H_∞ norm of the weighted frequency response. The majority of H_∞ techniques address a closed-loop system and the frequency response used for this exercise is that of the sensitivity function. The particular technique used for the gasifier problem is the H_∞ loop-shaping design procedure of MacFarlane and Glover [4] and Glover and MacFarlane [5]. This is unusual in that weighting function matrices are applied to the open-loop plant. This technique has the advantage of offering levels of robust performance, a stronger condition than that of robust stability.

As suggested above, the attainment of performance specifications depends on the selection of the weighting function matrices, denoted $\mathbf{W}_1$ and $\mathbf{W}_2$. It is through this selection process that the designer interacts with the design procedure. This procedure usually involves a degree of trial-and-error style iterative design. Various factors influence the choice of these weighting function matrices, such as the bandwidth, roll-off rate and low-frequency gain magnitude. Certain selection techniques require knowledge of the disturbance process to which the plant is subjected. Redefinition of the performance requirements may be necessary following an unsatisfactory outcome to the design procedure. The designer is faced with a number of considerations that must be balanced against one another in order to achieve the optimum trade-off between performance and robustness. Hence H_∞ optimization can be viewed as a multi-objective problem in itself.

1.2 Multi-objective optimization

Multi-objective optimization (MO) recognizes that most practical problems invariably require a number of design criteria to be satisfied simultaneously:

$$\min_{x \in \Omega} [f(x)] \quad (2)$$

where $x = [x_1, x_2, \ldots, x_q]$ and Ω define the set of free variables x subject to any constraints and $f(x) = [f_1(x), f_2(x), \ldots, f_n(x)]$ contains the design objectives to be minimized.

Clearly, for this set of functions $f_i(x)$, it is unlikely that there is one ideal 'optimal' solution, rather a set of Pareto-optimal solutions for which an improvement in one of the design objectives will lead to a degradation in one or more of the remaining objectives. Such solutions are also known as non-inferior or non-dominated solutions to the multi-objective optimization problem. An example of Pareto ranking for two objectives assuming a minimization problem is shown in Fig. 1. Individuals are ranked according to the number of individuals that show superior performance in terms of all the objectives. Hence, individual A is ranked 9 while individual B is ranked 0 and is referred to as non-dominated. (The box formed by connecting A to each of the objective axes contains nine solutions, all of which dominate A.)

Thus a multi-objective optimization strategy is compatible with the H_∞ controller design method. The inherent compromise between performance and robustness, which is prevalent in all control design approaches, lends itself to formulation as a multi-objective H_∞ optimization. Various specific performance criteria can be analysed in the context of how they affect the levels of stability. The ultimate task of the designer is to select a suitable controller from a range of non-dominated options. The population-based nature of genetic algorithms (GAs) offers an optimization strategy that can be adapted to perform within a multi-objective framework. Selection of the weighting function matrices $\mathbf{W}_1$ and $\mathbf{W}_2$ can be performed using this evolutionary technique and

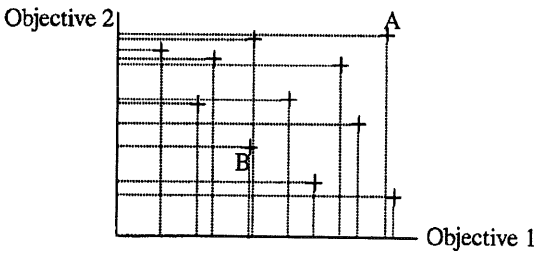

Fig. 1 Pareto ranking

the result assessed in terms of multiple performance objectives.

2 H_∞ LOOP-SHAPING DESIGN

The H_∞ loop-shaping design procedure is essentially a two-stage controller design technique [10]. Firstly, performance requirements are addressed by shaping the frequency response of the open-loop plant in a manner analogous to that of classical loop shaping. Secondly, robustness requirements are addressed using H_∞ optimization [10, 11] to stabilize the shaped plant, given a range of possible model uncertainty. The result is a single-degree-of-freedom controller, a configuration adequate for the disturbance rejection task of the challenge [1]. The design procedure assumes positive feedback in the closed-loop system.

2.1 Loop shaping

In classical linear single-input single-output (SISO) loop shaping, the magnitude of the open-loop transfer function is a function of frequency and is manipulated in order to meet system requirements. The gain of a multiple-input multiple-output (MIMO) plant, however, varies at any given frequency with the direction of the input vector. No unique gain value can be given for a multi-variable system as a function of frequency. A measure analogous to that of SISO plant gain is required for multi-variable systems if loop shaping is to be employed. Eigenvalues are unsuitable for this task as they provide only a measure of gain for the specific case of a square system whose input and output vectors are in the direction of an eigenvector. However, an accurate representation of the gain of a multi-variable system can be found using the singular value decomposition.

The singular value decomposition of any $l \times m$ matrix $\mathbf{G}$ can be written as

$$\mathbf{G} = \mathbf{U}\boldsymbol{\Sigma}\mathbf{V}^{\mathrm{H}} \tag{3}$$

where $\mathbf{V}^{\mathrm{H}}$ is the complex conjugate transpose of $\mathbf{V}$. Each column vector of matrix $\mathbf{U}$ represents the direction of the vector output signal produced by the plant $\mathbf{G}$ subject to an input in the direction of the corresponding column vector of matrix $\mathbf{V}$. These column vectors are each of unit length. $\boldsymbol{\Sigma}$ is a diagonal matrix of $\min\{l, m\}$ non-negative singular values in descending order of magnitude, the remaining diagonal elements being zero. These singular values represent the gain of $\mathbf{G}$ for the corresponding input and output directions in $\mathbf{V}$ and $\mathbf{U}$ and can be computed as the positive square roots of the eigenvalues of $\mathbf{G}^{\mathrm{H}}\mathbf{G}$.

$$\sigma_i(\mathbf{G}) = \sqrt{\lambda_i(\mathbf{G}^{\mathrm{H}}\mathbf{G})} \tag{4}$$

where $\sigma(\cdot)$ denotes a singular value and $\lambda(\cdot)$ denotes an eigenvalue. Hence the maximum singular value $\sigma_{\max}(\mathbf{G})$ and the minimum singular value $\sigma_{\min}(\mathbf{G})$ constitute the upper and lower bounds respectively on the range of system gains in response to all possible input directions at a given frequency.

In order to determine what constitutes a desirable shape for the plant singular values, the closed-loop configuration in Fig. 2 can be analysed. From this configuration the output y can be derived as being

$$y = (\mathbf{I} - \mathbf{G}_s\mathbf{K})^{-1}\mathbf{G}_s\mathbf{K}r + (\mathbf{I} - \mathbf{G}_s\mathbf{K})^{-1}\mathbf{G}_d d + (\mathbf{I} - \mathbf{G}_s\mathbf{K})^{-1}\mathbf{G}_s\mathbf{K}n \tag{5}$$

where r is the reference signal, d is the disturbance, n is the measurement noise, u is the plant input, y is the actual output and y_m is the measured output.

From equation (5) it can be seen that, when $|\mathbf{G}_s\mathbf{K}|$ is large, reference signals are propagated while disturbances are attenuated. However, a large value of $|\mathbf{G}_s\mathbf{K}|$ fails to subdue measurement noise and a trade-off situation arises. A compromise can be found because reference signals and disturbances are usually low-frequency events while measurement noise is prevalent over a much wider bandwidth. Acceptable performance can therefore be attained by shaping the singular values of $\mathbf{G}_s\mathbf{K}$ to give a high gain at low frequencies for disturbance rejection and a reduced gain at higher frequencies for noise suppression [10, 12].

For this particular design procedure, the purpose of

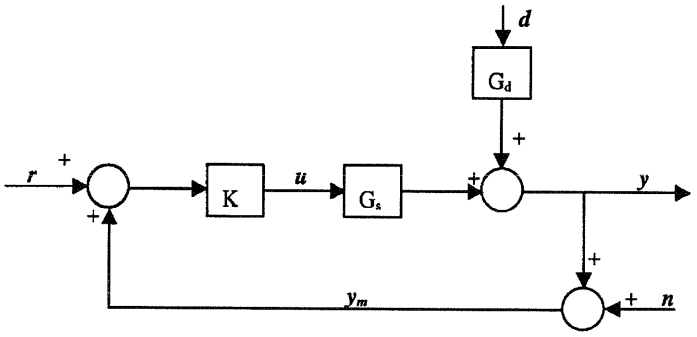

Fig. 2 One-degree-of-freedom feedback control system

K is to stabilize robustly the shaped plant as described in the next section; this shaping procedure cannot be accomplished through the manipulation of **K**. Hence $\mathbf{G}_s$ is defined to be the augmented plant $\mathbf{G}_s = \mathbf{W}_2\mathbf{G}\mathbf{W}_1$, where **G** represents the fixed plant. This structure allows the designer to shape the singular values of the augmented plant $\mathbf{G}_s$, through the selection of appropriate weighting matrices $\mathbf{W}_1$ and $\mathbf{W}_2$. The selection of these matrices is therefore the key element in attaining the performance requirements of the system and is the focal point of this design technique. This design task will be performed using a MOGA as outlined in Section 3.1.

2.2 H_∞ robust stabilization

The normalized left coprime factorization of a plant **G** is given by $\mathbf{G} = \mathbf{M}^{-1}\mathbf{N}$. A perturbed plant model $\mathbf{G}_p$ is then given by

$$\mathbf{G}_p = (\mathbf{M} + \Delta\mathbf{M})^{-1}(\mathbf{N} + \Delta\mathbf{N}) \tag{6}$$

To maximize this class of perturbed models such that the configuration shown in Fig. 3 is stable, a controller $\mathbf{K}_s$ that stabilizes the nominal closed-loop system and minimizes γ must be found, where

$$\gamma = \left\| \begin{bmatrix} \mathbf{K}_s \\ \mathbf{I} \end{bmatrix} (\mathbf{I} - \mathbf{G}\mathbf{K}_s)^{-1}\mathbf{M}^{-1} \right\|_\infty \tag{7}$$

This is the problem of robust stabilization of normalized coprime factor plant descriptions [**5**]. From the small-gain theorem [**10**], the closed-loop plant will remain stable if

$$\left\| \begin{bmatrix} \Delta\mathbf{N} \\ \Delta\mathbf{M} \end{bmatrix} \right\|_\infty < \gamma^{-1} \tag{8}$$

The lowest possible value of γ and hence the highest achievable stability margin is given by $\gamma_{\min} = [1 + \rho(ZX)]^{1/2}$, where ρ is the spectral radius, and Z and X are the solutions to the following algebraic Riccati equations:

$$(\mathbf{A} - \mathbf{B}\mathbf{S}^{-1}\mathbf{D}^{\mathrm{T}}\mathbf{C})Z + Z(\mathbf{A} - \mathbf{B}\mathbf{S}^{-1}\mathbf{D}^{\mathrm{T}}\mathbf{C})^{\mathrm{T}} - Z\mathbf{C}^{\mathrm{T}}\mathbf{R}^{-1}\mathbf{C}Z + \mathbf{B}\mathbf{S}^{-1}\mathbf{B}^{\mathrm{T}} = 0 \tag{9}$$

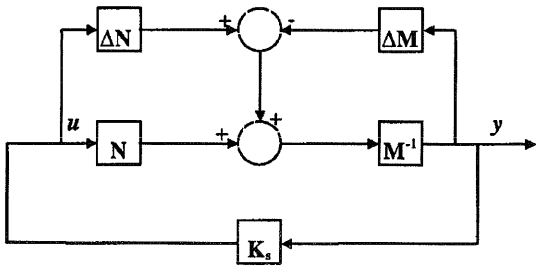

Fig. 3 Robust stabilization with respect to coprime factor uncertainty

$$(\mathbf{A} - \mathbf{B}\mathbf{S}^{-1}\mathbf{D}^{\mathrm{T}}\mathbf{C})^{\mathrm{T}}X + X(\mathbf{A} - \mathbf{B}\mathbf{S}^{-1}\mathbf{D}^{\mathrm{T}}\mathbf{C}) - X\mathbf{B}\mathbf{S}^{-1}\mathbf{B}^{\mathrm{T}}X + \mathbf{C}^{\mathrm{T}}\mathbf{R}^{-1}\mathbf{C} = 0 \tag{10}$$

where **A**, **B**, **C** and **D** are the state-space matrices of **G** and

$$\mathbf{R} = \mathbf{I} + \mathbf{D}\mathbf{D}^{\mathrm{T}}, \qquad \mathbf{S} = \mathbf{I} + \mathbf{D}^{\mathrm{T}}\mathbf{D} \tag{11}$$

By solving these equations, the state-space controller $\mathbf{K}_s$ can be generated explicitly [**10**]. This controller gives no guarantee of the system's performance, simply that it is robustly stable. It is therefore necessary to shape the system's response with both pre-plant weighting function matrix $\mathbf{W}_1$ and post-plant weighting function matrix $\mathbf{W}_2$ shown in Fig. 4. This will ensure that the closed-loop performance meets the specifications required.

3 MULTI-OBJECTIVE OPTIMIZATION USING GENETIC ALGORITHMS

The GA is a stochastic global search method which employs a Darwinian survival of the fittest principle. At each generation a population of potential solutions is assessed in terms of their performance in the problem domain. These individuals are then ranked according to their performance, the fittest having the highest probability of breeding. Pairs of individuals are then chosen according to these probabilities and bred together. Their offspring form the subsequent generation of potential solutions. A mutation operator is also implemented randomly in order to ensure that the probability of searching any given section of the search space is never zero. As this cycle repeats over a number of generations, the population becomes more refined as the least-fit individuals are rejected and an optimal solution is approached. The steps involved in the execution of a GA can be summarized as follows:

1. The genotypic representation, often encoded in binary, of an initial population is randomly generated.
2. These genotypic representations are converted to the corresponding phenotypes or decision variables.
3. The performance of each member of the population is assessed in turn using a prescribed objective function [**6**].

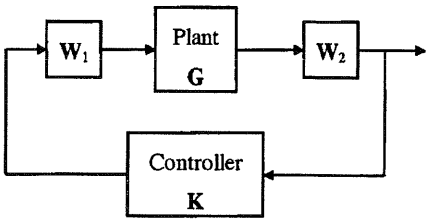

Fig. 4 Loop-shaping controller structure

4. Each individual is assigned a fitness value according to its objective function value.
5. Individuals are selected for reproduction according to a stochastic selection procedure with probabilities derived from their fitness function values.
6. Individuals genotypic representations are bred using specified mechanisms such as crossover.
7. A mutation operator is then applied stochastically to the genotypic representations of the offspring in order to ensure that the probability of investigating any given area of the search space is never zero.
8. The newly generated population is then assessed according to its objective function performance, the GA operations are repeated and new generations evolved until termination criteria are satisfied.

3.1 Multi-objective genetic algorithms

The MOGA is implemented using a standard GA [6] with extensions for multi-objective ranking, fitness shearing and mating restrictions. The salient features of MOGA are shown in Fig. 5 and described below.

Multi-objective ranking is based on the concept of the dominance of an individual and can be described by the scheme in Fig. 1. This system of ranking is non-unique, e.g. a number of individuals are ranked zero and these are said to be non-dominated. Ranking may also be combined with goal and/or priority information to discriminate between non-dominated solutions. For example, a solution in which all the goals are satisfied may be considered superior, or preferable, to a non-dominated solution in which the goal points of some objectives are not met [6]. All the preferred individuals thus achieve the same fitness; however, the number of actual offspring may differ due to the stochastic nature of the selection mechanism. Thus an accumulation of the imbalances in reproduction can cluster the search into an arbitrary area of the trade-off surface. This phenomenon is known as genetic drift and can drastically reduce the quality and efficiency of the search. Proposed as a solution to genetic drift, fitness sharing penalizes the fitness of individuals in popular neighbourhoods in favour of more remote individuals of similar fitness [6].

Recombining arbitrary pairs of non-dominated individuals can result in the production of an unacceptably high number of unfit offspring, or lethals. A further refinement to the MOGA is therefore to bias the manner in which individuals are paired for recombination, often termed mating restriction. This restricts reproductions to individuals that are within a given distance of each other. Population diversity is maintained by adding random genetic information at each generation as well as mutating existing individuals (see Add Random Immigrants in Fig. 5).

A MOGA was used to produce a population of potential solutions for the gasifier problem. Each solution consisted of a set of matrix elements for the pre-plant weighting matrix $\mathbf{W}_1$ and the post-plant weighting matrix $\mathbf{W}_2$. The use of the MOGA provided the means of implementing a multi-objective controller design strategy in contrast with other H_∞ and GA approaches which do not provide the designer with a visualization of the trade-off surface [13].

4 APPLICATION OF THE DESIGN TECHNIQUE TO THE GASIFIER PROBLEM

The flow chart in Fig. 6 provides an overview of the steps involved in the controller design process. A more specific discussion of the technique as applied to the gasifier is also given.

The MOGA tool was implemented using the MATLAB GA toolbox [14]. In order for the MOGA to rank the prospective controllers, and objective function vector tailored to the specific performance requirements of the gasifier is required. In order to evaluate each set of possible weighting matrix elements the objective function first has to construct the H_∞ controller by solving the algebraic Riccatti equations (9) and (10) using the 100 per cent load linear model of the gasifier. The weighting function structures used were those of a diagonal matrix of first-order lags for $\mathbf{W}_1$ and a diagonal matrix of gains for $\mathbf{W}_2$. The first-order lag structure of $\mathbf{W}_1$ was considered necessary to break any algebraic loop which may appear in simulation due to the non-zero $\mathbf{D}$ matrix in the linear model. The linear models of the gasifier contained 25 states and this design technique produces controllers which are at least of the order of the plant. The terms in $\mathbf{W}_2$ were specified as stateless in order to

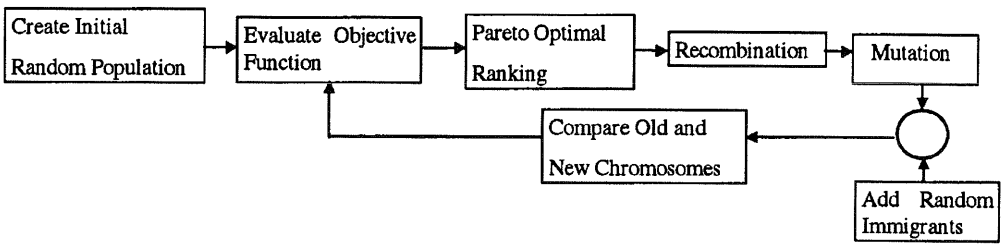

Fig. 5 The MOGA

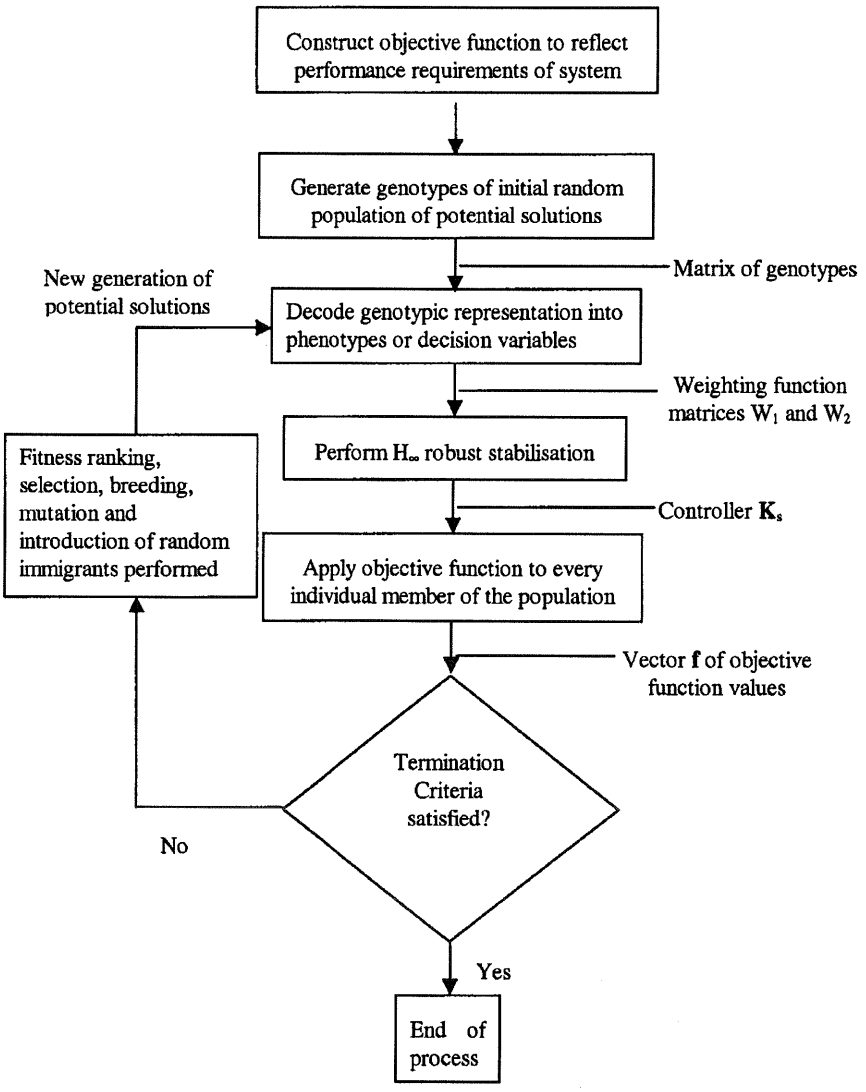

Fig. 6 Flow chart of the MOGA H_∞ controller design process

minimize the order of the resultant controllers. Each controller's performance was then evaluated by running a simulation on the 100 per cent load model subject to a step and a sine wave disturbance as specified in the challenge [1]. As the optimization philosophy of MOGA is to minimize objective function values, the plant model was not offset, relative values about the operating point being preferred to absolute input–output values. This allowed the objective function to assess the peak deviations in gasifier outputs produced by each candidate controller by taking the maximum absolute value of each output vector. Input constraints were observed by placing saturation and rate-limit blocks on the inputs of the SIMULINK system representation containing relative values appropriate to the operating point. The minimization of the integral of absolute error (IAE) of each output was also specified as a design objective. In the case of the gas quality and pressure outputs the IAE was minimized in order to encourage a short settling time and to reduce steady state error while in the case of the bed mass and temperature outputs, the aim was to prevent a possible violation of the output constraints beyond the stipulated 300 s run time of the test simulation. Stability of the closed-loop system was guaranteed by optimizing the maximum closed-loop continuous eigenvalue and discarding any individual in the population which did not result in a maximum closed-loop eigenvalue less than zero. One further objective attempted to minimize the H_∞ norm γ in order to maximize the robustness of the closed-loop control system.

Figure 7 shows a typical parallel coordinates trade-off for the gasifier. The ten objectives shown in Table 1 are identified along the x axis. Each line represents the performance in the objective domain of a potential solution (one individual), i.e. the performance arising from a set of weighting matrix elements. The crosses which are

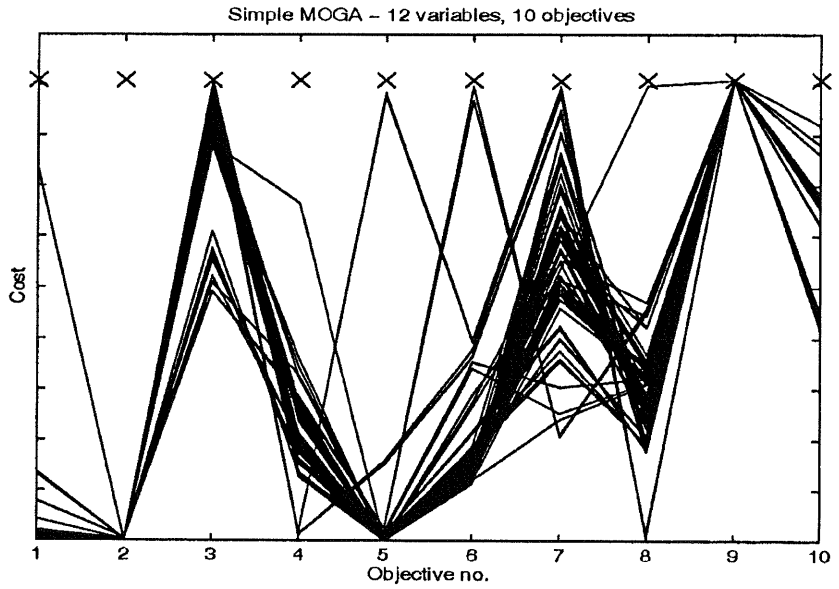

Fig. 7 Trade-off graph

Table 1 Objectives

Objective	Objective description
1	Peak fluctuation of CVGAS from the operating point
2	Peak fluctuation of MASS from the operating point
3	Peak fluctuation of PGAS from the operating point
4	Peak fluctuation of TGAS from the operating point
5	IAE of CVGAS over 300 s
6	IAE of MASS over 300 s
7	IAE of PGAS over 300 s
8	IAE of TGAS over 300 s
9	Maximum continuous eigenvalue of closed-loop system
10	H_∞ robustness measure γ

ranged across the graph denote the goal values for each objective. For example, objective 1 is to minimize the peak fluctuation of the fuel gas calorific value CVGAS from its operating point value. The cross is situated at the specified limit of 10 000 J/kg. Each line on the graph indicates the performance of the associated individual in relation to the corresponding objectives. It can clearly be seen that, for objective 1, all solutions have an objective value less than that of the goal value. This means that all potential controllers offered by the MOGA have been successful in containing the peak fluctuation of the calorific value to within $\pm 10\,000$ J/kg. Figure 8 also shows a situation in which all individuals perform successfully in relation to the performance specifications but the objectives have been reordered on the graphical user interface to enable comparison between adjacent objectives. The displayed ranges of each objective are normalized to leave the crosses representing the optimization goals near the top of the graph.

Competition between adjacent objectives is indicated by crossing lines whereas concurrent lines represent non-competing objectives. Here, the goals relating to maximum output fluctuation (objectives 1 to 4) are set to the limits stated in the challenge. These targets are specified as constraints in order to guarantee that controllers represented on the trade-off graph satisfy the output constraints over the run-time of the simulation. From Fig. 7 it can be seen that all the controllers represented here offer excellent control over peak bed mass fluctuation (objective 2). Therefore the bed mass peak fluctuation, as an objective, is not in competition with any other objective. However, the bed mass does trade off with the pressure in terms of the IAE of both outputs as shown by the lines crossing between objectives 6 and 7. There is also competition between the IAE of pressure and temperature (objectives 7 and 8). Concurrent lines between objectives 5 and 6 indicate that both calorific value and bed mass can be optimized simultaneously in terms of the IAE.

The objective visualization tool allows the objectives to be swapped around, producing alternative ordering of objectives. This provides the user with a representation more conducive to gaining insight into the trade-off surface. Further work is currently being undertaken to produce more advanced visualization techniques to quantify the degree of competition and to identify trade-off 'hot spots'. The peak fluctuation objective value of each output has been placed adjacent to its IAE in Fig. 8. Note that objectives 9 and 10 are not relevant to this study and are left untouched. This format allows assessment of whether the two measures of each output compete with each other. The vast majority of lines are, in fact, concurrent between the associated objectives. The controllers represented will therefore optimize both the peak fluctuation and the IAE of any chosen outputs.

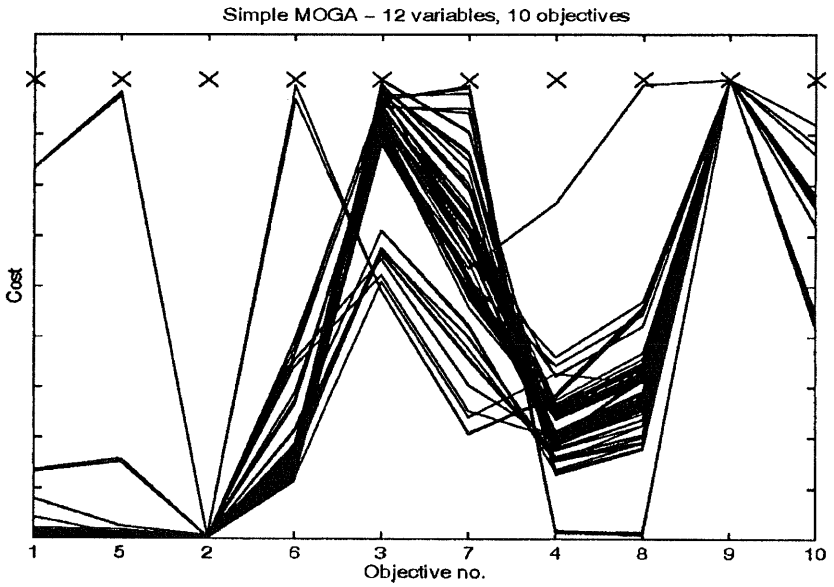

Fig. 8 Reordered trade-off graph

This makes the designer's tasks easier as a final controller selection based on only one of these performance measures can be made.

The final choice of controller was made with reference to both the performance requirements and the need for stability across all three operating points. As previously stated in Section 1, the properties of performance and robustness are always in competition during the process of control system design. The choice of controller for which results are shown below was considered to offer the best possible achievement of goal values while retaining stability across the entire operating range.

The design solutions shown in Fig. 7 achieved all the performance specifications at the 100 per cent load operating point as indicated by the fact that the lines are beneath the goal marker crosses. However, simulations showed that these solutions produced unstable or high-frequency oscillatory behaviour at the 0 per cent operating point. As this was considered unacceptable, the priority level of the most difficult objective, that relating to pressure, was relaxed from constraint to objective. This allowed a larger number of potential solutions to be considered and the final choice of controller came from the subset of potential solutions which were revealed by this priority change.

4.1 Mapping for the MOGA-tuned H_∞ method

Controller design specifications relating to system performance are often expressed in terms of time or frequency domain metrics which the resulting system is required to satisfy or exceed. Other desirable characteristics relating to the relative stability of the system and the achievable robustness may also be targeted. The multi-objective optimization approach to control system design used here expresses system requirements in terms of vectors of objectives and goals, the aim being to minimize the objective vector elements in accordance with the goal vector requirements. The mapping between these alternative expressions is shown in Fig. 9 and the design specifications can be found in reference [1].

4.2 Results

The results are shown in Figs 10 to 17.

4.3 Performance test figures

Tables 2 to 7 show the performance test figures. The values in parentheses indicate that a constraint violation has occurred.

4.4 Discussion of results

At the 100 per cent load operating point, the graphical results show that the controller exerts effective control over the calorific value, bed mass and temperature in terms of not exceeding the challenge's constraints when subjected to a step in the disturbance signal. The gas pressure is less effectively controlled as it can be seen to peak and settle outside the specified constraints. Steady state errors are present at all four outputs, the magnitudes of these being relatively small for all except the pressure. Extended run-time simulations show that these steady state errors remain constant and do not tend towards the set point.

In the case when the sinusoidal disturbance is applied

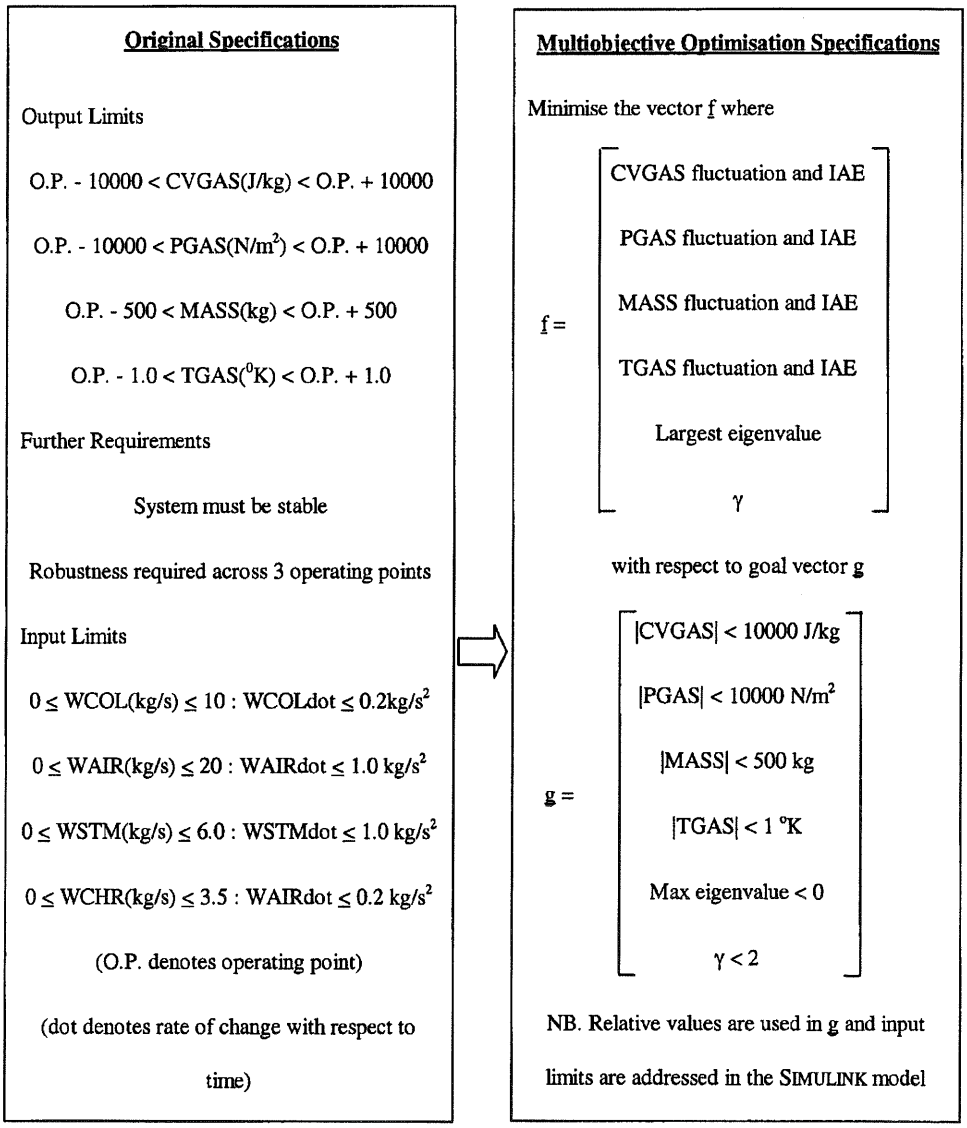

Fig. 9 Mapping of system specifications into multi-objective formulation

to the 100 per cent loading operating point, control can be seen to be more effective in terms of not violating the challenge's constraints. All four outputs remain within their specified limits and extended run-time simulations show that this situation continues beyond 300 s.

The step disturbance applied to the 0 per cent load operating point results in control performance similar to that of the step at the 100 per cent operating point. Again, there are no constraint violations for calorific value, bed mass and gas temperature and these responses demonstrate small steady state errors. Again the signals result in steady state errors during extended run-time simulations. The gas pressure, however, can be seen both to peak and to settle beyond the constraints set by the challenge as in the 100 per cent case.

The response to a sinusoidal disturbance at the 0 per cent load operating point differs from that at the 100 per cent operating point. While the calorific value, bed mass and gas temperature remain within their constraints, the gas pressure exceeds both the maximum and the minimum constraint values.

Results show a robust, stable, controller design capable of exerting effective control over three of the four outputs across all three operating points. The control exerted over the gas pressure is, however, not sufficiently effective to satisfy the requirements of the challenge at any of the operating points.

The design procedure outlined above evolves a number of potential controllers. For example, alternative solutions which exert tighter control over pressure at the expense of calorific value constraint violations can also be produced. The design procedure has been shown to

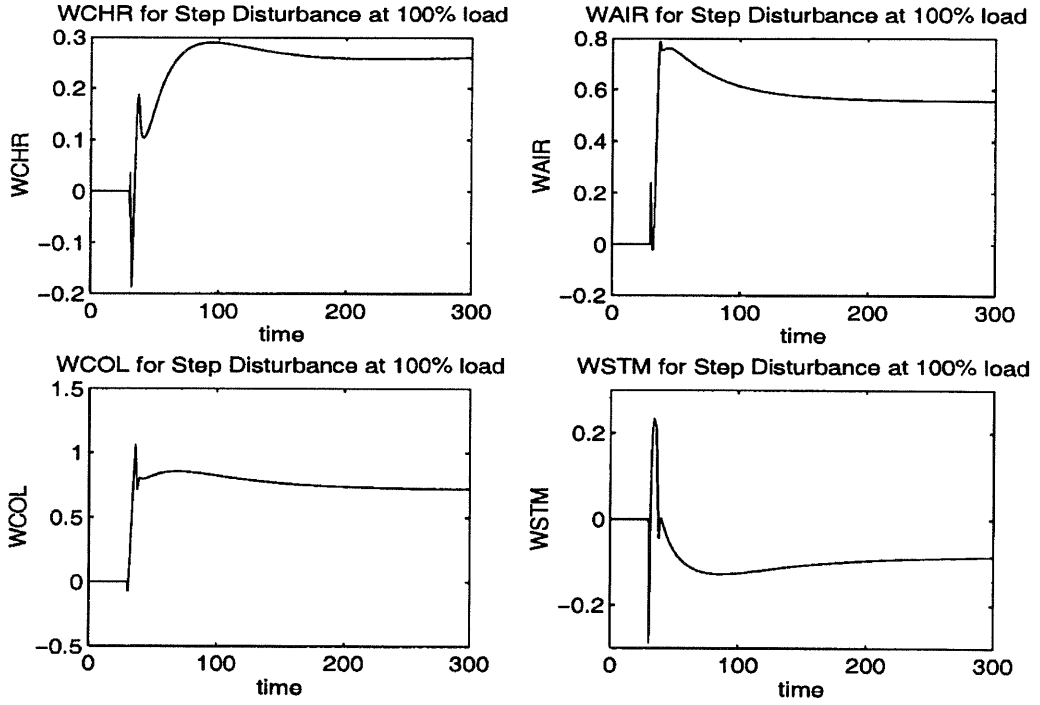

Fig. 10 Plant inputs resulting from a step disturbance at 100 per cent load

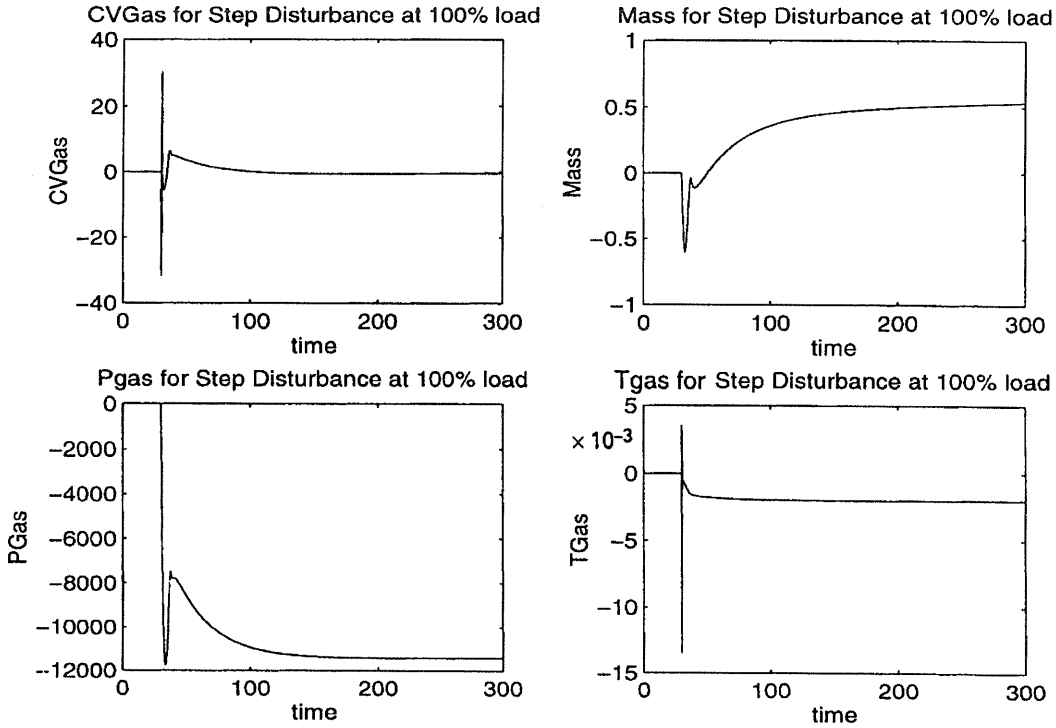

Fig. 11 Plant outputs resulting from a step disturbance at 100 per cent load

be capable of fulfilling the performance requirements of all four outputs across two of the three operating points. However, in this particular case, stability was not achieved for the 0 per cent load operating point. Potential alternatives to the results presented in Section 4.3 demonstrate that the procedure evolves a family of solutions, allowing the designer to analyse various permutations of achievable performance before

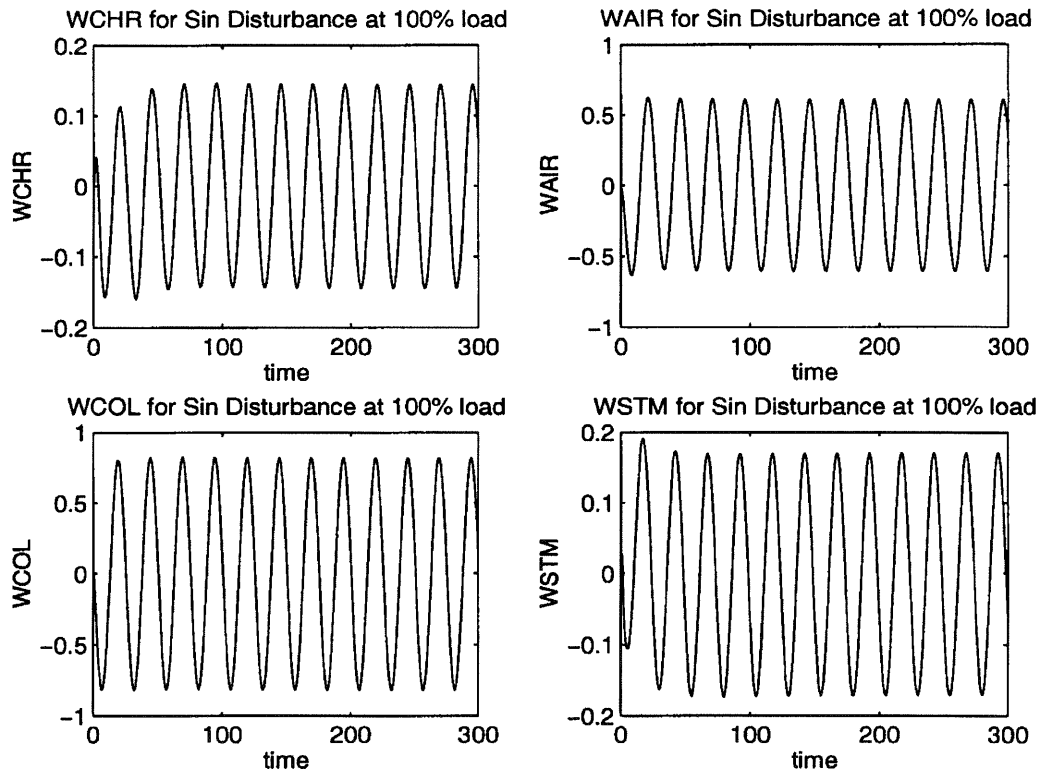

Fig. 12 Plant inputs resulting from a sine wave disturbance at 100 per cent load

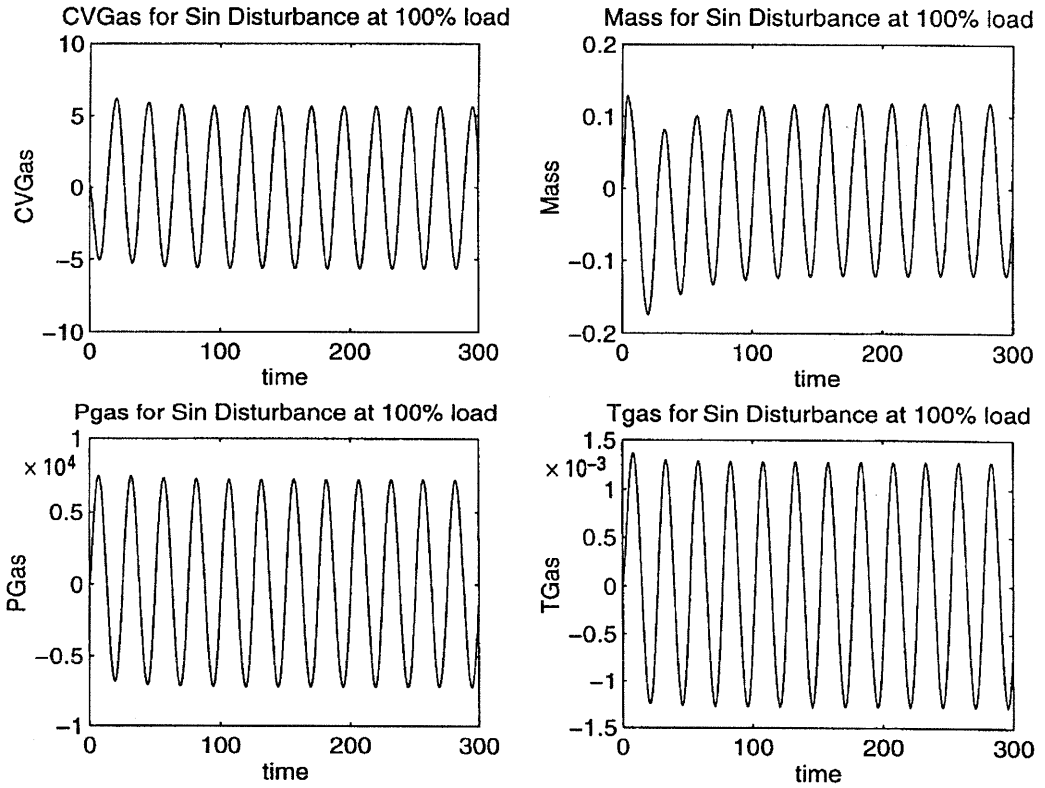

Fig. 13 Plant outputs resulting from a sine wave disturbance at 100 per cent load

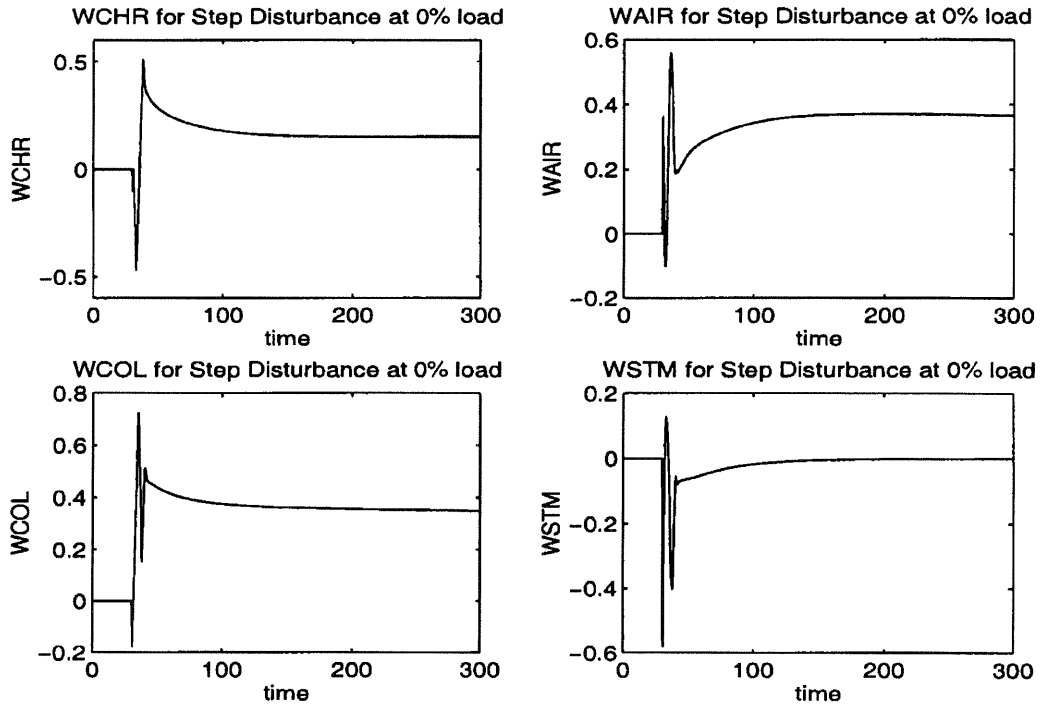

Fig. 14 Plant inputs resulting from a step disturbance at 0 per cent load

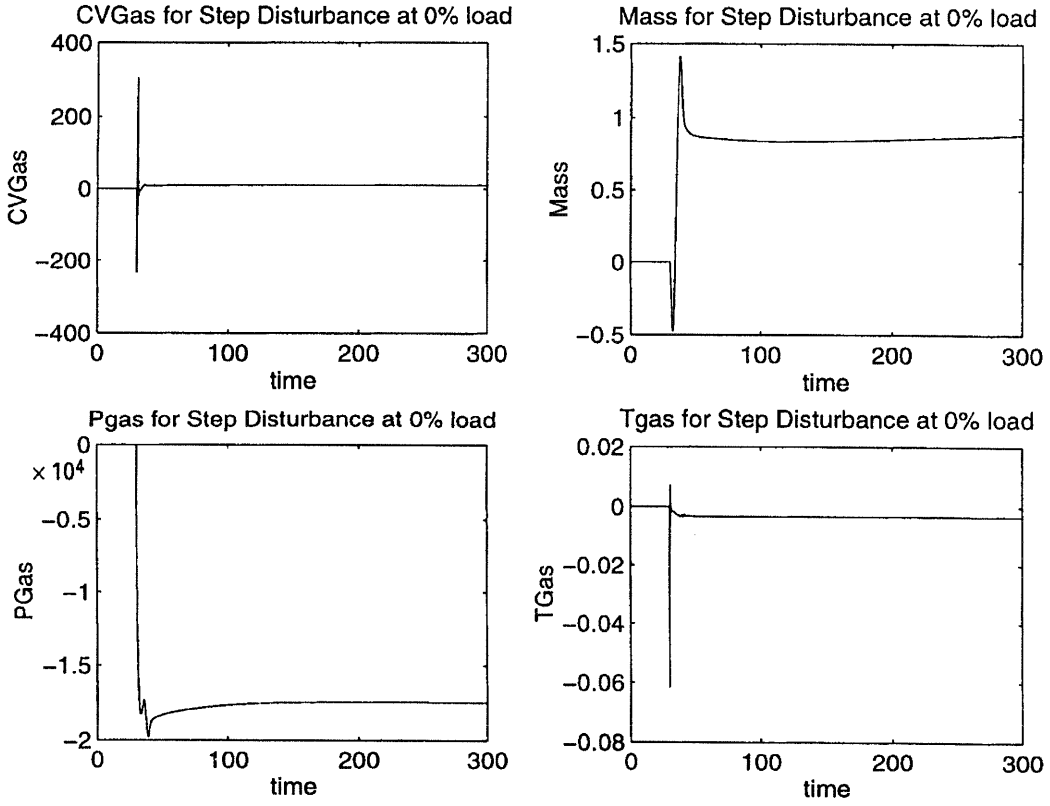

Fig. 15 Plant outputs resulting from a step disturbance at 0 per cent load

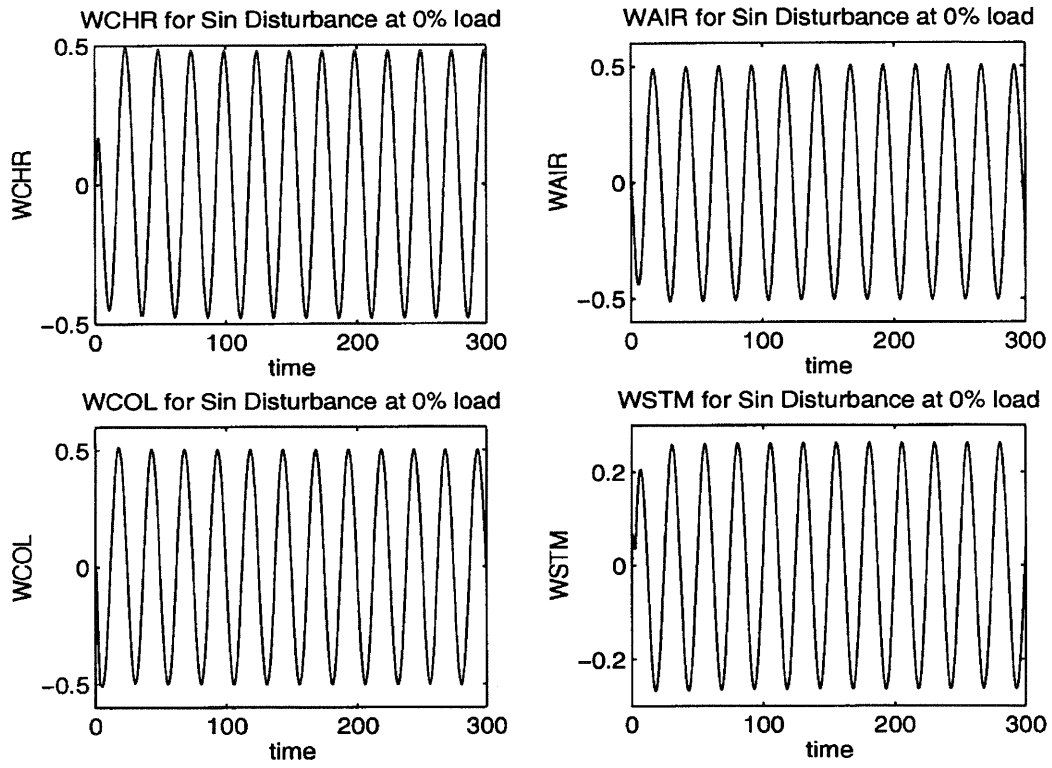

Fig. 16 Plant inputs resulting from a sine wave disturbance at 0 per cent load

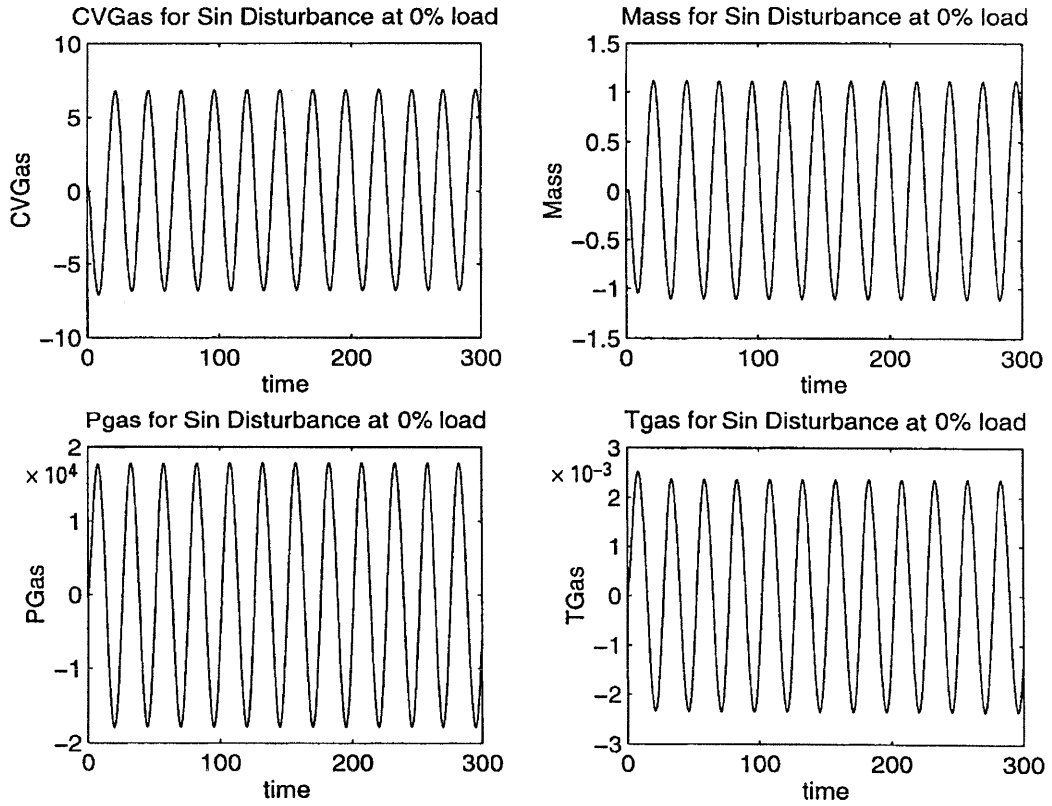

Fig. 17 Plant outputs resulting from a sine wave disturbance at 0 per cent load

Table 2 Performance figures produced with a step disturbance at 100 per cent load operating point

	Maximum and minimum absolute values			
	Maximum	Minimum	Peak rate	IAE
Inputs				
WCHR	1.19	0.71	0.2	—
WAIR	18.2	17.4	1	—
WCOL	9.61	8.48	0.2	—
WSTM	2.93	2.41	1	—
Outputs				
CVGAS	$4.360\,030\,25 \times 10^6$	$4.359\,968 \times 10^6$	7.603×10^2	2.6288×10^2
MASS	$1.000\,053 \times 10^4$	9.9994×10^3	0.35	—
PGAS	200 000 0	$(1.988\,248\,6 \times 10^6)$	$8.069\,95 \times 10^3$	$2.945\,501 \times 10^6$
TGAS	1.2232×10^3	$1.223\,19 \times 10^3$	0.21	—

Table 3 Performance figures produced with a sine wave disturbance at 100 per cent load operating point

	Maximum and minimum absolute values			
	Maximum	Minimum	Peak rate	IAE
Inputs				
WCHR	1.05	0.74	0.05	—
WAIR	18.04	16.79	0.16	—
WCOL	9.37	7.73	0.2	—
WSTM	2.89	2.53	0.09	—
Outputs				
CVGAS	$4.360\,006\,2 \times 10^6$	$4.359\,994\,3 \times 10^6$	3.01	1.0756×10^3
MASS	$1.000\,013 \times 10^4$	9.9998×10^3	0.06	—
PGAS	$2.007\,488\,75 \times 10^6$	$1.992\,763\,4 \times 10^6$	1.85×10^3	$1.383\,076\,6 \times 10^6$
TGAS	$1.223\,20 \times 10^3$	$1.223\,198\,7 \times 10^3$	4.78×10^{-4}	—

Table 4 Performance figures produced with a step disturbance at 50 per cent load operating point

	Maximum and minimum absolute values			
	Maximum	Minimum	Peak rate	IAE
Inputs				
WCHR	1.32	0.72	0.2	—
WAIR	11.78	10.89	1	—
WCOL	6.52	5.34	0.2	—
WSTM	1.86	1.37	1	—
Outputs				
CVGAS	$4.490\,040\,5 \times 10^6$	$4.489\,970\,6 \times 10^6$	1.0495×10^3	2.1639×10^2
MASS	$1.000\,064 \times 10^4$	$9.999\,63 \times 10^3$	0.27	—
PGAS	1 550 000	$(1.537\,396\,6 \times 10^6)$	9.955×10^3	$3.025\,637\,7 \times 10^6$
TGAS	1.1811×10^3	$1.181\,08 \times 10^3$	0.37	—

making the final choice of controller. This is a key strength of the MOGA approach as the various design objectives do not have to be prioritized *a priori*.

5 CONCLUSIONS

An evolutionary algorithm approach has been proposed for the H_∞ design of a coal burning gasification plant. The resulting controller has satisfied a number of conflicting design criteria typically imposed on such a critical system. The control system has been shown to be stable across all three operating points, maintaining the fluctuation of the gas calorific value, temperature and bed mass within stated limits. However, effective control of the gas pressure in terms of the constraints on signal fluctuation specified by the Challenge was not achieved even at the design point.

It has subsequently been shown that the controller design procedure described above is capable of providing improved control performance for the ALSTOM gasifier problem from that presented here. The design procedure

Table 5 Performance figures produced with a sine wave disturbance at 50 per cent load operating point

	Maximum and minimum absolute values			
	Maximum	Minimum	Peak rate	IAE
Inputs				
WCHR	1.31	0.46	0.1	—
WAIR	11.61	10.16	0.19	—
WCOL	6.45	4.23	0.2	—
WSTM	1.89	1.5	0.3	—
Outputs				
CVGAS	$4.490\,009 \times 10^6$	$4.489\,993\,4 \times 10^6$	35.53	9.5636×10^2
MASS	$1.000\,02 \times 10^4$	$9.999\,77 \times 10^3$	0.1	—
PGAS	$(1.560\,161\,68 \times 10^6)$	$1.540\,008\,5 \times 10^6$	2.6232×10^3	$1.896\,876 \times 10^6$
TGAS	1.1811×10^3	1.1811×10^3	6.9×10^{-4}	—

Table 6 Performance figures produced with a step disturbance at 0 per cent load operating point

	Maximum and minimum absolute values			
	Maximum	Minimum	Peak rate	IAE
Inputs				
WCHR	1.01	0.03	0.2	—
WAIR	4.9	4.24	1	—
WCOL	2.86	1.96	0.2	—
WSTM	0.8	0.09	1	—
Outputs				
CVGAS	$4.710\,304\,7 \times 10^6$	$4.709\,767 \times 10^6$	3.239×10^3	2.6431×10^3
MASS	1.0001×10^4	$9.999\,53 \times 10^3$	0.53	—
PGAS	1 120 000	$(1.100\,250\,1 \times 10^6)$	1.7617×10^4	$4.743\,26 \times 10^6$
TGAS	1.1151×10^3	1.115×10^3	0.959 54	—

Table 7 Performance figures produced with a sine wave disturbance at 0 per cent load operating point

	Maximum and minimum absolute values			
	Maximum	Minimum	Peak rate	IAE
Inputs				
WCHR	0.99	0.02	0.12	—
WAIR	4.84	3.83	0.16	—
WCOL	2.65	1.63	0.2	—
WSTM	0.94	0.41	0.16	—
Outputs				
CVGAS	4.71×10^6	$4.709\,992\,8 \times 10^6$	3.61	$1.305\,39 \times 10^3$
MASS	$1.000\,11 \times 10^4$	9.999×10^3	0.28	—
PGAS	$(1.137\,82 \times 10^6)$	$(1.102\,096 \times 10^6)$	$4.479\,59 \times 10^3$	$3.402\,65 \times 10^6$
TGAS	1.1151×10^3	1.1151×10^3	0.001	—

can be modified to address specifically the robustness issues involved in applying the same linear controller to a wide operating envelope. The number of objectives used by the MOGA was extended from 10 to 14. This enabled the peak fluctuation of each output to be assessed at each operating point while still retaining the minimization of the largest closed-loop eigenvalue and the measure of H_∞ robustness as design objectives. The minimization of the IAE of each output was not addressed in this modified design procedure. Control performance was shown to be much improved as a result of these modifications with the gas pressure only violating the constraints at the 0 per cent load operating point. Steady state errors did, however, remain as in the results presented here. For a full account of this improved design procedure, see reference [**15**].

It should be noted that the mixed optimization approach allows other design parameters to be included in the problem formulation. For example, the IAE of all four outputs were declared as explicit design criteria.

The evolutionary algorithm approach to controller design employed here is advantageous in that the result is that the designer has a choice of controllers rather than one specific design. The final selection between various performance characteristics can be made in the knowledge that all comply with the restrictions imposed on the system. The trade-off graph informs the designer of the implications that his or her choice will have on all the explicit design objectives. The approach automated the process of selection of suitable weighting functions, searching a wider range of options than would normally be contemplated when using conventional techniques. A particularly strong feature of the GA approach is the ability to use a mixture of discrete and continuous parameters in the problem formulation. This leads to an intuitive and natural representation for the problem being considered and simplifies the process of efficiently searching a large space.

One limitation of this approach is that it addresses a very specific formulation of the design problem. While the response of the chosen controller may be optimal in terms of the objectives expressed, there is no guarantee that its performance will be acceptable in other scenarios. Use of the design technique therefore requires careful selection of design objectives and *a posteriori* simulation testing.

REFERENCES

1 **Dixon, R., Pike, A. W.** and **Donne, M. S.** The ALSTOM benchmark challenge on gasifier control. *Proc. Instn Mech. Engrs, Part I, Journal of Systems and Control Engineering*, 2000, **214**(I6), 389–394.

2 **Zakian, V.** Critical systems and tolerable inputs. *Int. J. Control*, 1989, **49**(4), 1285–1289.

3 **Whidborne, J. F.** and **Lui, G. P.** *Critical Control Systems: Theory, Design and Applications*, 1993 (Research Studies Press, Baldock, Hertfordshire).

4 **MacFarlane, D. C.** and **Glover, K.** *Robust Controller Design Using Normalised Coprime Factor Plant Descriptions*, Lecture Notes on Control and Information Science, Vol. 138, 1990 (Springer-Verlag, Berlin).

5 **Glover, K.** and **MacFarlane, D. C.** Robust stabilisation of normalised coprime factor plant descriptions with H_∞ bounded uncertainties. *IEEE Trans. Autom. Control*, 1989, **34**(8), 821–830.

6 **Fonseca, C. M.** and **Fleming, P. J.** An overview of evolutionary algorithms in multiobjective optimisation. *Evolutionary Computation*, 1993, **1**(1), 25–49.

7 **Walker, D. J.** and **Postlethwaite, I.** Advanced helicopter flight control using two-degree-of-freedom H_∞ optimisation. *J. Guidance, Control and Dynamics*, 1996, **19**(2), 461–468.

8 **Young, J. S.** and **Lin, C. E.** Refined optimal approach to rotorcraft flight control—a simulation on time responses. In Proceedings of the First IEEE Conference on *Control Applications*, Bath, 1992, Vol. 2, pp. 818–824.

9 **Hyde, R. A.** and **Glover, K.** The application of scheduled controllers to a VSTOL aircraft. *IEEE Trans. Autom. Control*, 1993, **38**(7), 1021–1039.

10 **Skogestad, S.** and **Postlethwaite, I.** *Multivariable Feedback: Control, Analysis and Design*, 1996 (John Wiley, Chichester, West Sussex).

11 **Williams, S. J.** H_∞ for the layman. *Measmt Control*, 1991, **24**(2), 18–21.

12 **Maciejowski, J. M.** *Multivariable Feedback Control*, 1989 (Addison-Wesley, Workingham, Berkshire).

13 **Chen, B. S.** and **Cheng, Y. M.** A structure-specified H_∞ optimal control design for practical applications: a genetic approach. *IEEE Trans. Control Systems Technol.*, 1998, **6**(6), 707–718.

14 **Chipperfield, A. J., Fleming, P. J.** and **Pohlheim, H. P.** A genetic algorithm toolbox for MATLAB. In Proceedings of the International Conference on *Systems Engineering*, Coventry, September 1994, pp. 200–207.

15 **Griffin, I. A.** and **Fleming, P. J.** Multiobjective optimisation approach to gasifier control. Research Report 777, Department of Automatic Control and Systems Engineering, University of Sheffield, 2000.